Evidence for Angular Effects in Proton-Induced Single-Event Upsets

Robert A. Reed, *Member, IEEE*, Paul W. Marshall, *Member, IEEE*, Hak S. Kim, *Member, IEEE*, Peter J. McNulty, *Member, IEEE*, Bryan Fodness, *Member, IEEE*, Tom M. Jordan, *Member, IEEE*, Ron Reedy, *Member, IEEE*, Chuck Tabbert, *Member, IEEE*, Mike S. T. Liu, *Member, IEEE*, Walter Heikkila, *Member, IEEE*, Steve Buchner, *Member, IEEE*, Ray Ladbury, *Member, IEEE*, and Kenneth A. LaBel, *Member, IEEE*

***Abstract*—Historically, proton-induced single-event effects (SEEs) ground test data are collected independent of the orientation of the microelectronic device to the proton beam direction. In this study, we present experimental and simulation evidence that shows an effect of over an order of magnitude on the proton-induced single-event upset (SEU) cross section when the angle of incidence of the proton beam is varied. The magnitude of this effect is shown to depend on the incidence proton energy and the device critical charge. The angular effect is demonstrated for Silicon-On-Sapphire and Silicon-On-Insulator technologies, but would not necessarily be limited to these technologies.**

I. Introduction

In 1975, Bender *et al.* [1] published the first results that demonstrated that it was possible to induced a change in the logic state of a microelectronic device by a single particle irradiation, known as single-event upset (SEU). Over the 27 years following that study, experimental and modeling investigations on the effects of single ionizing particle events on microcircuits has uncovered many effects, all of which are grouped into single-event effects (SEEs). This long history has led to a traditional approach for proton-induced SEU ground testing that ignores the directionality of the incident proton relative to the sensitive volume. Also, most on-orbit rate predictions techniques do not consider the direction of the incident proton.

Manuscript received July 16, 2002. This work was supported in part by the NASA NEPP/ERC Project and the Defense Threat Reduction Agency.

R. A. Reed and K. A. LaBel are with the NASA Goddard Space Flight Center, Greenbelt, MD 20771 USA (e-mail: robert.a.reed.1@gsfc.nasa.gov).

P. W. Marshall is with Goddard space Flight Center, Greenbelt, MD 20771 USA.

H. S. Kim is with Jackson and Tull Chartered Engineering, Washington, DC 20018 USA (e-mail: hkim@pop700.gsfc.nasa.gov).

P. J. McNulty is with Clemson University, Clemson, SC 29634 USA.

B. Fodness is a NASA/GSFC Support Contractor with SGT Inc., Greenbelt, MD 20770 USA.

T. M. Jordan is with EMPC, Gaithersburg, MD 20885 USA.

R. Reedy and C. Tabbert are with Peregrine Semiconductor, Melbourne, FL 32901 USA.

M. S. T. Liu and W. Heikkila are with Honeywell SSEC, Plymouth, MN 55441 USA.

S. Buchner is a NASA/GSFC Support Contractor with QSS Inc., Seabrook, MD 20706 USA.

R. Ladbury is with Orbital Sciences, Inc., NASA Goddard Space Flight Center, Greenbelt, MD 20771 USA (e-mail: rladbury@pop500.gsfc.nasa.gov).

Digital Object Identifier 10.1109/TNS.2002.805446

In [2]–[4], we published series of papers showing that the proton-induced SEU cross section could depend on the angle of incidence of the proton beam relative to the sensitive volume (SV). The angular effect was partially attributed to the forward directed nature of recoiling nuclei that result from a spallation reaction between the incident proton and the silicon nucleus. We studied, via simulations, the implications of SV geometry and device critical charge. The general results are as follows.

1) The angular effect depends heavily on the device critical charge. A device with higher critical charge is more sensitive to angular effects.
2) Angular effects can exist if the sensitive volume has at least one thin dimension compared to the other dimensions.
3) As geometries become smaller, the angular effect increases.

Prior to this study, conclusive experimental confirmation of this angular effect has not been published; however, suggestive indications were presented in [5] and [6], and they are summarized below.

SEU cross-section data were published in [5] on a Matra HM65656 SRAM. The data show a factor of 2 to 4 increase as a function of proton-beam angle of incidence going from normal to grazing. In [7], we presented data on the Matra HM65656 that did not show an angular effect.

Data on an SOI device were given in [6] that showed over an order of magnitude variation in the SEU cross section when the proton beam angle was varied. However, the error bars on these data were over an order of magnitude.

In this paper, we continue our investigation on proton-induced angular effects on SEU cross section by presenting experimental results that clearly demonstrate the angular effect does exist, and may be widespread and significant. We present data taken on two different technologies: a Silicon-On-Sapphire (SOS) process from Peregrine Semiconductor and Silicon-On-Insulator (SOI) process from Honeywell SSEC. These data show that the angular effect can be over an order of magnitude. This will have a significant impact on the on-orbit SEU rate and the test methods and calculational tools used to compute this rate.

We also present new experimental and simulation results that demonstrate that the magnitude of the angular effect will depend strongly on the proton energy and device critical charge.

II. Mechanisms That Induce an Angluar Effect

Spallation reactions, nuclear elastic collisions, and direct ionization are the three dominant mechanisms for proton-induced SEU. What follows is a brief discussion developed from [8]–[14] that focuses on these mechanisms and the implications of proton beam angle of incidence on SEU ground measurements.

A. Nuclear Scattering

The dominant mechanism for SEUs occurring in devices with linear energy transfer (LET) >1.0 MeV•cm^2/mg will either be elastic nuclear scattering, spallation reactions, or some combination of these. The detail depends on the incident proton energy and the device critical charge. Comparing the nuclear cross section for each mechanism at the test energy helps to define the dominant mechanism.

Spallation reactions products dominate the SEU response for proton energies >50 MeV. For example, for 63-MeV protons, the interaction cross section for producing a recoil from an elastic scattered recoil atom that has a LET >3.0 MeV•cm^2/mg is more than a factor of 6 lower than that for spallation reactions (which tend to have higher LETs and longer ranges) [14]. This factor grows to more than an order of magnitude for LETs >5.0 MeV•cm^2/mg.

However, for 30-MeV protons, the nuclear elastic recoil production probability for LETs >3 MeV•cm^2/mg is only a factor of two less than the probability of producing a spallation reaction, and for LETs >5 MeV•cm^2/mg, it is less than a factor of 6 [14]. It is interesting to note that 30-MeV protons are common in the radiation environment for many space flight applications.

The final observation is that the angular dependence can be complicated by the fact that the spallation reaction recoils tend toward the path of the initial proton trajectory, while direction of the recoils from elastic scattering tend to be perpendicular to the trajectory except for the more energetic recoils. This fact can also be used as an indicator of the mechanism that is producing SEUs, as will be seen later.

B. Direct Ionization

Direct ionization will most likely be the dominant mechanism for devices with LET thresholds <1.0 MeV•cm^2/mg, depending on proton energy. The impact of increased energy deposited via direct ionization when the proton beam is rotated can be easily assessed if the normal incident heavy ion threshold LET (LET$_c$) is known.

Assume that LET$_c$ is constant over the SV thickness (t) traversed by normally incident heavy ions. The energy deposited during a near grazing event is the integral of the proton LET over the path length (Y). Then the minimum path length required to cause an upset can be found by solving this equation for Y

$$\mathrm{LET}_c \times t = \int_0^Y \mathrm{LET}_{\mathrm{proton}}\, dt. \tag{1}$$

For constant LET$_{\mathrm{proton}}$, the path length through the SV must be greater than the ratio of LET$_c$ to the LET$_{\mathrm{proton}}$. It is interesting to note that for 200-MeV proton and a LET$_c$ $=$ 1.0 MeV•cm^2/mg, this ratio is nearly 270. But, for 15-MeV protons and the same critical charge, this ratio is near 17. The aspect ratio of many SOI and SOS technologies can be much greater than 17. However, these technologies typically have threshold LETs much great than 1.0 MeV•cm^2/mg. This type of "litmus test" calculation could be an indicator that a technology exhibit enhancement from proton-induced direct ionization.

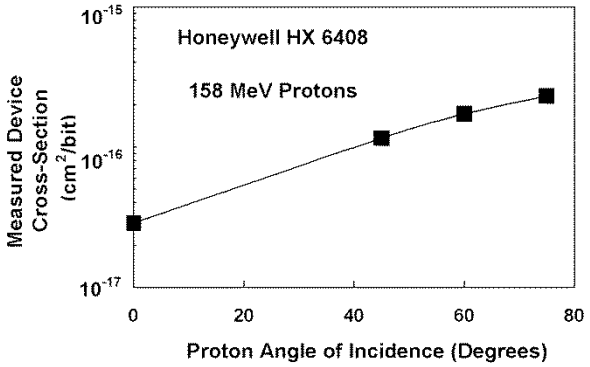

Fig. 1. Measured device SEU cross-section results for the HX6408 when exposed to 158-MeV protons. Notice the order of magnitude increase in the cross section near 75° (near gazing angle to the die surface).

III. Experimental Results and Discussion for the Honeywell SSEC SOI SRAM

A. Honeywell SOI SRAM and Test Setup

The Honeywell HX6408 is a 512 k $\times$ 8 Static RAM fabricated in Radiation Insensitive CMOS V (RICMOSV) 0.35-μm SOI process. The process is a SOI CMOS technology with an 80 angstrom gate oxide and a 4000 angstrom buried oxide. The silicon under the gate is 0.21 μm thick. For the n-channel FET, the gate length is 0.35 μm and the width is 1 μm.

The SRAM device is designed using a seven-transistor memory cell that operates at 3.3 V. Testing was carried out using the test methods described in [15].

B. Measure Proton Induced Angular Dependence for Memory Cell Single-Event Upsets

Data were collected on the HX6408 at Indiana University Cyclotron Facility (IUCF) using 158-MeV protons. (The data were collected by Honeywell SSEC.) The device was operated at a supply bias of 3.3 V. Four irradiations were carried out with proton-beam angles of incidence set at 0, 40, 60, and 73°. The data showing the variation of the SEU cross section per bit over proton angle of incidence are given in Fig. 1. Zero degrees corresponds to the proton beam being incident normal to the large surface area of the die, and 90° is at grazing angle to the die surface (this definition of angle is used throughout the paper). Note the increase of over an order of magnitude in the device SEU cross section at 73° versus 0°.

Data were also taken for 40-MeV protons at IUCF. The measured SEU cross section when protons were incident normal to the die surface was 1×10^{-17} cm^2/bit and increased to near 9×10^{-17} cm^2/bit at 73°.

The maximum error cross section for the HX6408 cannot be determined using the traditional approach for collecting data

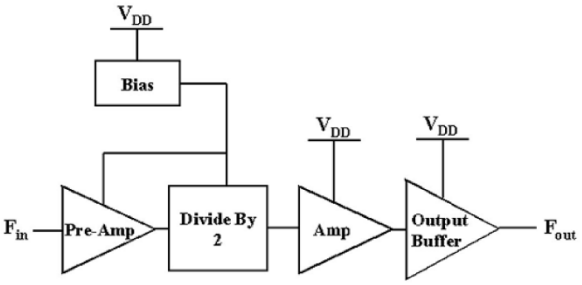

Fig. 2. Block diagram of Peregrine PE9301 2- to 3.5-GHz prescaler.

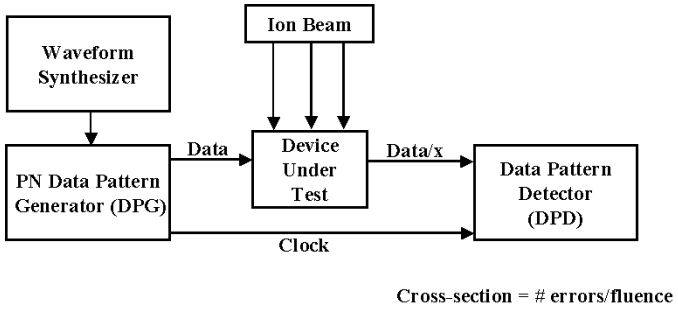

Fig. 3. Test setup for testing the PE9301.

(e.g., data collection with the proton beam normally incidence to the die surface). Collecting data at normal incidence would lead to an underestimation of the on-orbit error rate. As such, the increased error rate could significantly impact spacecraft on-orbit performance. This angular effect will be observed on other devices.

C. Mechanisms for Inducing the Observed Angular Effect

Proton-induced direct ionization cannot cause SEUs in this device. Using (1), the heavy-ion LET response curve data from [15], and setting $t = 0.21$ μm (the thickness of the silicon under the gate) gives that a 158-MeV proton would need to traverse the SV over 150 μm to cause an upset via direct ionization. Given that the largest transistor size is 1 μm, direct ionization cannot cause the angular effect.

For 158-MeV protons, the probability for an elastic scatter to produce a recoil with sufficient energy to upset the device is more than an order of magnitude less than the probability for spallation reactions [14]. Spallation reactions dominate the SEU response and cause the angular effect.

IV. Experimental Results and Discussion for 63 MeV Proton Exposures of a SOS Prescaler

A. Peregrine PE9301 Prescaler

The Peregrine Semiconductor divide-by-two prescaler is fabricated in Ultra Thin Silicon (UTSi) 0.5-μm SOS process. For this technology, the silicon under the gate is about 980 angstrom thick, with about 20 angstrom standard deviation, wafer to wafer and across a wafer. For PE9301 devices, the gate length is 0.5 μm and gate width varies throughout the design from about 1.5 μm up to 10 μm.

A block diagram of Peregrine's PE9301 high-speed prescaler is shown in Fig. 2. The prescaler core, a true single phase clock (TSPC) dynamic D flip-flop (DFF) with feedback is used to implement the divide-by-2 function. A pre-amp buffers the prescaler input before it is fed into the divider core. The pre-amp consists of a CMOS inverter with resistive feedback from output to input. Both the pre-amp and divide-by-2 core derive their bias from a current source set by on-chip resistors. These two blocks operate at a lower internal supply, which contributes to the design's power savings. The external supply is nominally at 3 V.

The amplifier that follows the divider core has three stages of buffering in order to drive the output stage. Finally, the output buffer consists of transistors connected in a push–pull configuration to drive a 50-ohm load.

Simulations including layout parasitic capacitances as well as package models predicted a maximum operating frequency of 5.7 GHz under nominal condition (3-V supply and room temperature). The recommended operation range is from 2.0 to 3.5 GHz.

B. Test Setup for Peregrine Prescaler

The SEU testing was done using the BA3600 bit error rate tester (BERT) from SyntheSys Research, Inc. (see Fig. 3). The BERT generates the input pattern to the device under test (DUT) and detects errors on the DUT output. The data pattern generator (DPG) and data pattern detector (DPD) are independent on the BA3600. A Hewlett Packard waveform synthesizer from (HP83712B) provides the input clock frequency to the BA3600.

The DPG generated a square-wave data signature with 50% duty cycle at the frequency of the waveform synthesizer. These data are passed to the prescaler, which divides the input by two. The output of the prescaler is passed to the DPD for error detection and error signature storage. The expected data pattern from the prescaler is captured prior to irradiation and stored in DPD so that it can be used to detect errors in the prescaler output during an irradiation. The DPG also provides the clock input to the DPD.

Once optimization was reached, the DUT was placed in the particle beam and the DPD continuously compared the data pattern from the DUT against the expected pattern. For all mismatches, the error signatures were recorded along with their locations in the data stream. Consecutive mismatches of 100 or more are considered to be a synchronization error. When this occurred, an automatic synchronization was initiated and achieved by the DPD. The data storage capability of the BA3600 allowed the data to be categorized and tallied into synchronization errors or bit error events. Bit error events are those that have error signatures lengths less than 100.

C. Error Modes for Peregrine Prescaler

Small spot size laser testing at the NRL Laser Facility [16] showed that synchronization errors occurred only when laser was placed in the area of the die that contained the pre-amp or the DFF, exposing other areas of the die did not induce synchronization errors. Events in the pre-amp or the DFF act as an extra clock signal, causing the data to lose synchronization with the clock. Laser testing also showed that bit error events are induced

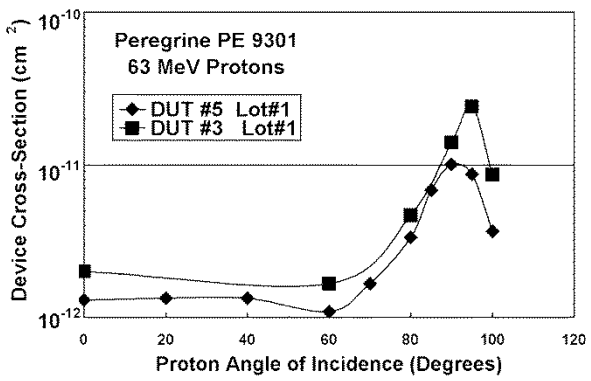

Fig. 4. Measured device SEU cross-section results for the PE9301 when exposed to 63-MeV protons. Notice the order of magnitude increase in the SEU cross section near 90° (grazing angle to the die surface).

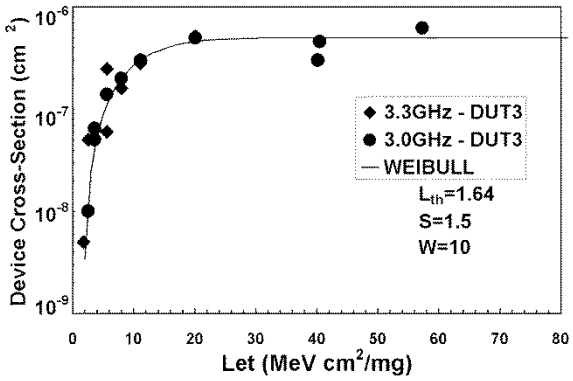

Fig. 5. Measured heavy ion SEU cross-section results for the PE9301.

in the amplifier, output buffer, and a small portion of the DFF. These errors do not cause a loss of synchronization of the BERT.

D. Angular Dependence Data for Prescaler Bit Error Events for 63-MeV Protons

Data were taken on the PE9301 prescaler at the University of California at Davis (UCD) using a 63-MeV proton beam. (The data were collected by NASAS/GSFC.) For all tests, the device was operated at an input power of 0 dBm at 3.3 GHz, and the supply bias was set at 3.0 V. Several irradiations were carried out at various proton-beam angles of incidence for two DUTs. Fig. 4 gives the device SEU cross-section results over proton angle-of-incidence for bit error events. (Zero degrees correspond to the proton beam being incident normal to the die.) The data show an increasing SEU cross section at angles $>60°$, with an increase of over an order of magnitude at grazing angles.

Just like the Honeywell SRAM, the maximum value in the error cross section for this device cannot be determined using the traditional data collection approach. This increase in SEU cross section would significantly impact on-orbit performance and rate predictions.

During these tests, the device was exposed to a total fluence that exceeded 6×10^{13} p/cm^2; we observed only two synchronization errors. Also, there was no observable change in the device performance—the device performed nominally after begin exposed to 6×10^{13} p/cm^2 (note that we did not perform a complete parametric evaluation). We verified that the SEU cross section did not change after these high fluence exposures by periodically remeasuring the SEU cross section using the identical parameters used for the first measurement. Each check showed no change in the measured SEU cross section.

Data collected when the prescaler was exposed to 200-MeV protons will be presented later in this paper. Also later in the paper, we will present data collected on two Peregrine prescalers that have identical designs but have different critical charges.

E. Mechanisms for Inducing the Observed Angular Effect

Heavy ion data can be used to rule out direct ionization as the cause of the angular effect. We performed heavy ion measurements on the prescaler at Texas A&M University Cyclotron. The bit error event data at 3.3 and 3.0 GHz is shown in Fig. 5. (As with the proton data, the synchronization error cross section was very low, $<2 \times 10^{-8}$ cm^2/device for LETs >11 MeV•cm^2/mg. We did not observe synchronization errors below this LET.)

These data show significant fall off the SEU cross section at an LET of 2.5 MeV•cm^2/mg. Using LET$_c = 0.58$ MeV/μm in (1), and letting $t = 0.098$ μm (the thickness of the silicon under the gate), we find that a 63-MeV proton would need to traverse the SV over 30 μm to cause an upset via direct ionization. Given that the largest transistor size is 10 μm, it is very unlikely that direct ionization is the cause of this angular effect.

Again, the dominant mechanism is spallation reaction. The discussion in Section II finds that for 63 MeV, the probability for an elastic scatter to induce an upset is more than a factor of six less than the probability for spallation reactions [14].

The experimental data agree with this prediction. Given that the 0.098-μm thin layer of silicon is coplanar to the die surface and there is very little or no charge that is collected from 250-μm-thick sapphire layer, the large area of the SV is coplanar to the die surface. The longest path length through the SV is parallel to the die surface. So, the longest path length for spallation recoils is when the proton beam is at grazing angles to the die surface, while the longest path lengths for elastic scatter recoils are when the proton beam is normal to the die surface. The measured SEU data show an increase near grazing angles (see Fig. 4), implying that spallation reactions are the cause of the angular effect.

We note that for 30-MeV protons, there will be a mixing of the effects that corresponds to a more closely to a proportion of two-thirds spallation reactions and one-third nuclear elastic scatters. We predict that this mixing of the mechanisms will complicate the measured angular effects.

V. Impact of Proton Energy on the Angular Effect for the Peregrine Prescaler

Proton energy can have a significant effect on the measured SEU cross section [8] as well as having an impact on the magnitude of the effect that proton beam angle-of-incidence has on measure SEU cross section.

A. Experimental Results

Fig. 6 plots the normalized device SEU cross section as a function of proton beam-angle of incidence for 63-MeV and

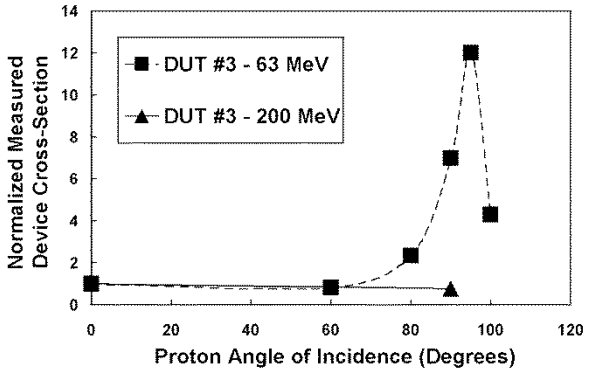

Fig. 6. Normalized measured SEU cross-section data for the PE9301 for 63- and 200-MeV protons. Note the angular dependence disappears for the 200-MeV case.

200-MeV protons for the Peregrine PE9301 prescaler. (The 200-MeV data were collected at IUCF by NASA/GSFC using the setup described in Section IV.) The SEU cross-section data are normalized to the 0° data. DUT #3 was used for all data collection. The shape of the SEU cross section over angle depends on incident proton energy. The data at 63 MeV shows an increase for angles greater than 60, while there is no angular effect for the 200-MeV exposures.

B. Discussion of the Energy Dependence

The variation in the angular dependence under exposure to different proton energies can be understood by comparing the angular distribution of the spallation recoils for 63-MeV protons to that for 200-MeV protons. The GEANT simulation tool [12] was used to compute the angular distribution of the recoiling nucleus's energy, range, and LET.

Fig. 7 gives simulation results for 63- and 200-MeV protons incident on a silicon target. There are six panels, the left side is for 63-MeV protons and the right side is for the 200-MeV case. For each side, the top panel is the angular distribution (relative to the incident proton trajectory) of the energy of the recoiling nucleus; the middle panel is the LET distribution for the recoil nuclei and the third is the recoil nuclei range distribution (LET and range are for Si). The angle is the deflection of the recoiling nucleus away from the initial primary proton trajectory.

For either energy case, the most energetic recoils (longest range, highest LET) are forward directed and are the most frequently occurring events. Also note that the lower energy recoils (shortest range, lower LET) are more isotropic.

Recall that the threshold LET for the Prescaler is near 2.5 MeV•cm^2/mg. The data in Fig. 7 show that the events are more isotropic for the 200-MeV case than for the 63-MeV case when the LET $<$ 6 MeV•cm^2/mg. The anisotropic distribution of recoil nuclei causes the angular effect observed at 63 MeV, while at 200 MeV, the angular effect will be more isotropic. This agrees with the energy dependence seen in the experimental data in Fig. 6.

C. Modeling the Proton-Induced SEU Response

1) CUPID Simulation Tool: Energy deposition in a SV from nuclear spallation reaction products must be modeled if the SEU

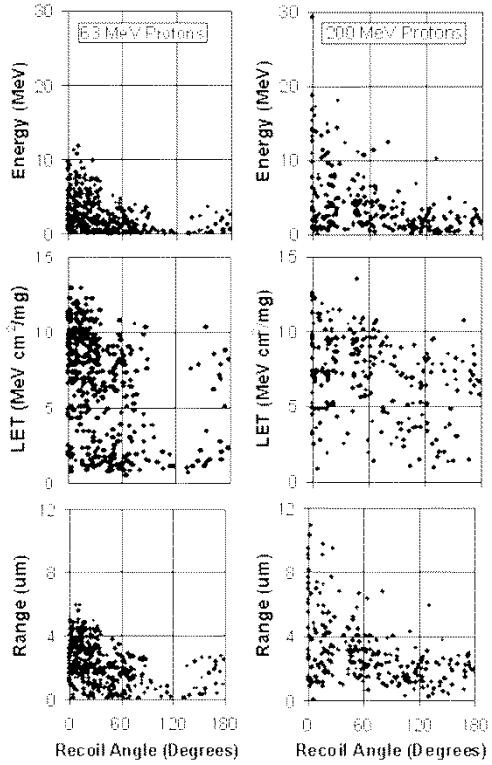

Fig. 7. Distribution of spallation reaction recoil energy, LET, and range in Silicon for 63- and 200-MeV protons.

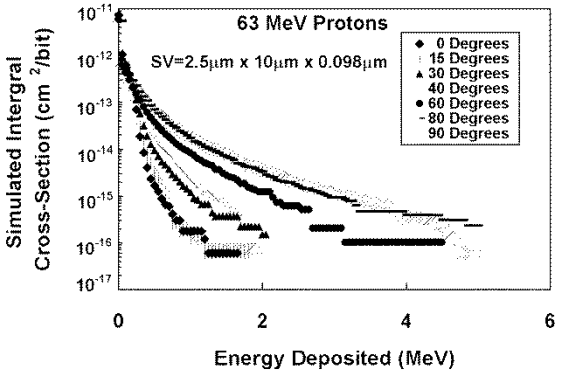

Fig. 8. CUPID simulation results for integral cross section for 63-MeV protons.

response of the Peregrine Prescaler is to be modeled. There are several computer codes for simulating proton-induced spallation reactions [12], [17]–[19]. We chose to use the Clemson Omni-directional Spallation Model for Interaction in Circuits (COSMIC) [4], which extends the Clemson University Proton Interactions in Devices (CUPID) [19] Monte Carlo simulation tool to allow for various angles of incidence exposures. The CUPID/COSMIC codes were developed to compute the integral cross section for events depositing a threshold amount energy in a SV by a series of spallation reactions products.

The inputs to the code are the right rectangular parallelepiped sensitive volume dimensions, the incident proton energy, and the proton-beam angle of incidence relative to the SV.

Fig. 8 gives a set of typical CUPID/COSMIC results, where the 63-MeV protons were incident on a 2.5 $\times$ 10 $\times$ 0.098 μm^3

SV. The simulations were done such that all events occurring within a volume size of 22.5 × 30 × 20.098 μm^3 were included. The SV was located at the center of this volume. The integral cross section for depositing a certain amount of energy or greater is plotted as a function of the energy deposited. The simulations were carried out for 0, 15, 30, 40, 60, 80, and 90° rotation. The rotation is the angle between the proton trajectory and the normal to the 2.5 × 10-μm^2 area, rotated toward the 10-μm side. Notice that the cross section increases with increasing angle of incidence for energy deposition greater than about 0.2 MeV, qualitatively in agreement with the experimental data.

In the next two sections, we will use these types of simulation results to model the SEU response of the Peregrine prescaler over angle and proton energy.

2) Modeling Assumption for the Peregrine SOS Prescaler: For PE9301 devices, the gate length is 0.5 μm and the gate width varies throughout the design from about 1.5 μm up to 10μm.

The average amount of energy that must be deposited (ED_{ave}) to cause an upset is estimated by finding the LET at 50% of the saturated SEU cross section. The data in Fig. 5 and a SV thickness of 980 angstrom (thickness of the silicon under the gate) give ED_{ave} for DUT#3 to be 0.3 MeV.

In [20] and [21], the authors show that for some thin buried-oxide SOI technologies, significant charge collection can come from the region below the buried oxide, extending the thickness of the sensitive volume. So simply assuming the dimension of the volume of silicon under the gate is probably not accurate for these thin devices. For the Peregrine SOS technology, the sapphire layer is ∼250 μm after back lapping. So charge collection from below the sapphire layer is not possible and there is no enhancement to the SV thickness from effect.

It is less straightforward to determine the SV area. Laser testing (Section III-C) showed that almost every block within the prescaler has transistors that can induce bit error events. There are multiple SVs throughout the device and the SV areas for these vary in size, depending on which transistor size is sensitive. The transistor sizes in the prescaler vary from 0.5 × 1.5 μm^2 to 0.5 × 10 μm^2. The gate width varies from 1.5 to 10 μm. So, we let one side of the SV area be defined by the minimum or the maximum transistor gate width.

We know that there are approximately 20 gates used to build up the device. The average area of the SV can be determined from the heavy ion saturated SEU cross section (Fig. 5). This gives the average SV area of 3 μm^2.

A series of CUPID/COSMIC simulation were carried out to understand the implication of having a distribution of SVs with various geometries. We assumed a SV area range from 0.5 × 1.5 μm^2 to 2.5 × 10 μm^2. We observed less than 20% variation in the normalized SEU cross sections over this range, indicating that the angular dependence can be estimated from any of these geometries. The simulated SEU cross sections were normalized to the value at 0°.

3) CUPID Modeling Results: Fig. 9 plots the normalized simulated cross section, normalized to the value at 0°, for 63-MeV and 200-MeV simulations for two SVs, 2.5 × 10 × 0.098 μm^3 and 2.5 × 1.5 × 0.098 μm^3. (The format used throughout this paper for defining the rotation is $SV = L \times W \times T$, and the rotation is done about an axis parallel to W.) The simulations accurately predict the energy dependence given by the experimental data (Fig. 6) at 90° and at 0°.

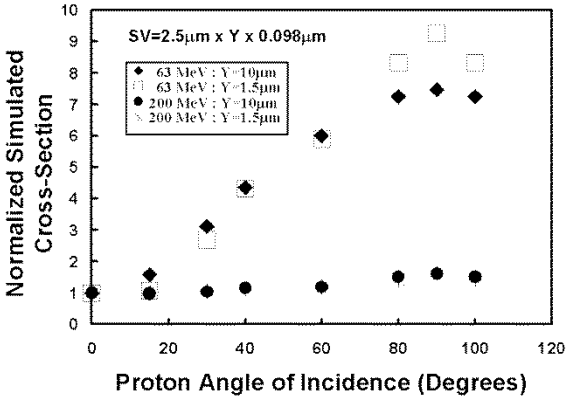

Fig. 9. Normalized CUPID prediction for the angular and energy dependence. The simulation agree to first order; however, there is a discrepancy between 30° and 75°.

For 63 MeV, the predictions agree well with the experimental data near 90°. However, the simulations over estimate the ratio for angles between 30° and 75°. CUPID is a p + Si reaction code. It assumes that all elements in the SV and surrounding volume are silicon. In reality, when protons are incident normal to the die, the recoils are primarily a result of interactions with elements in the gate and the silicon under the gate (elements that are very similar in Z to silicon). But, when rotated to some angle there are other materials that are in the path, (e.g., contribution from oxygen in the SiO_2 and the elements that make up sapphire). CUPID does not take these into account. This is most likely the cause of the disagreement between the experimental data and the simulations. This modeling would require a tool like GEANT that can model various elements as the target material.

VI. Impact of Critical Charge on the Angular Effect for the Peregrine Prescaler

In [2] and [3], we predicted that the critical charge would have an impact on the SEU cross section's angular dependence.

We received two different lots from Peregrine that were fabricated from the same mask set but with very different process parameters. DUT #3 and #5 were from very early process runs. DUT #114 was manufactured ∼1.5 years later, after several process changes had occurred. Fig. 10 shows the normalized measured SEU cross section for 63-MeV exposures at UC Davis for the two devices. The angular dependence for DUT#114 is not as clearly evident as that for DUT#3.

Laser testing at NRL Laser Facility showed that the laser threshold for bit error events for DUT#114 was approximately 50% lower than that for DUT#3. Recall that DUT#3 $ED_{ave}$was 0.3 MeV. This implies that the ED_{ave} for DUT#114 would be as low as 2.0 MeV.

The effect of critical charge can be modeled for the Peregrine prescaler using CUPID simulation results for various energy depositions. Fig. 11 plots normalized simulated cross section for various threshold energy depositions (ED) for a $SV =$

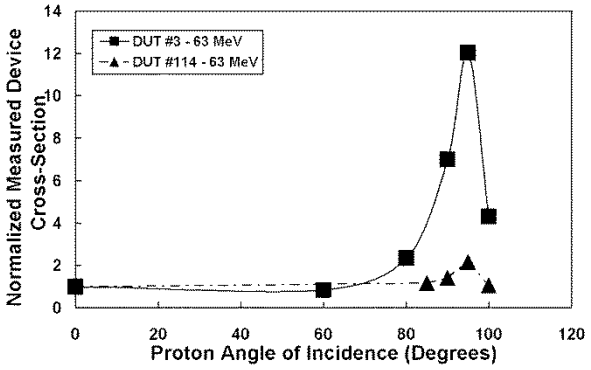

Fig. 10. Normalized measured SEU cross-section data for the PE9301 for DUTs 3 and 114. Note the angular dependence is less severe for DUT 114, which has a lower critical charge.

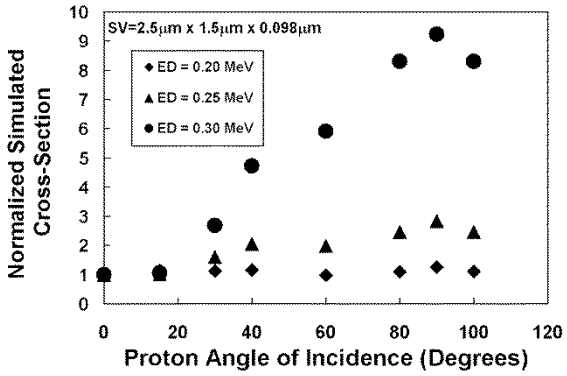

Fig. 11. Normalized CUPID prediction for the dependence on critical charge.

$2.5 \times 1.5 \times 0.098\ \mu\text{m}^3$. Lower EDs (or critical charge) yield a reduced dependence on angle of incidence.

The simulation results in Fig. 11 for ED between 2.0 and 2.5 MeV agree well with the experimental data for DUT#114 in Fig. 10.

VII. Conclusion

We have presented new experimental SEU data that show that SOI and SOS technologies can be sensitive to proton beam angle-of-incidence. The measured SEU cross sections for the Peregrine SOS technology had an angular enhancement between 2 and 12, depending on the proton energy and the device critical charge. The Honeywell SOI technology shows an enhancement factor of about nine for the test energies used.

The Honeywell device is a static SRAM and the Peregrine device is a high-speed prescaler, two very different circuits that are expected to have very different responses to radiation. The difference is evident by comparing the cross sections at a fixed angle (Figs. 1 and 4). The fact that the cross sections are much higher for the SOI device does not imply that SOI technology is more or less sensitive than SOS technology.

However, the two device do have one thing in common, they both show a dependence on the proton-beam angle of incidence. The large aspect ratio of the SVs in both technologies is the key common characteristic that produces the angular effect.

We also presented new simulation results based on actual device geometries that agree somewhat with experiments over energy and critical charge. Although the simulation did not agree with the data over all angles, it did estimate the maximum deviation accurately.

Our findings impact both test planning and rate prediction approaches, and indicate that present methods may underestimate observed upset rates by greater than $5\times$.

References

[1] D. Binder, E. C. Smith, and A. B. Holman, "Satellite anomalies from galactic cosmic rays," *IEEE Trans. Nucl. Sci.*, vol. NS-22, pp. 2675–2680, Dec. 1975.

[2] R. A. Reed, P. J. McNulty, and W. G. Abdel-Kader, "Implications of angle of incidence in SEU testing of modern circuits," *IEEE Trans. Nucl. Sci.*, vol. 41, pp. 2049–2054, Dec. 1994.

[3] R. A. Reed and P. J. McNulty, "Effects of geometry on the proton SEU dependence on the angle of incidence," *IEEE Trans. Nucl. Sci.*, vol. 42, pp. 1803–1808, Dec. 1995.

[4] R. A. Reed *et al.*, "A simple algorithm for predicting proton SEU rates in space compared to the rates measured on the CRRES satellite," *IEEE Trans. Nucl. Sci.*, vol. 41, pp. 2389–2395, Dec. 1994.

[5] F. Gardic *et al.*, "Analysis of local and global transient effects in a CMOS SRAM," in *Proc. RADECS'95*, 1995, pp. 346–353.

[6] F. Gardic *et al.*, "Dynamic single event effects in a CMOS/thick SOI shift register," in *Proc. RADECS'95*, 1995, pp. 333–339.

[7] R. A. Reed *et al.*, "Heavy ion and proton-induced single event multiple upset," *IEEE Trans. Nucl. Sci.*, vol. 44, pp. 2224–2229, Dec. 1997.

[8] P. E. Dodd, "Basic mechanisms for single event effects," in *Proc. IEEE Nuclear and Space Radiation Effects Conf.—Short Course*, 1999.

[9] W. J. Stapor, "Single-event effects qualification," in *Proc. IEEE Nuclear and Space Radiation Effects Conf.—Short Course*, 1995.

[10] E. L. Petersen, "Single event analysis and prediction," in *Proc. IEEE Nuclear and Space Radiation Effects Conf.—Short Course*, 1997.

[11] J. D. Kinnison, "Achieving reliable, affordable systems," in *Proc. IEEE Nuclear and Space Radiation Effects Conf.—Short Course*, 1998.

[12] (2002, June) Geant4 User's Manual: For Application Developers. [Online]. Available: http://wwwinfo.cern.ch/asd/geant4/G4UsersDocuments/UsersGuides/ForApplicationDevelopers/html/index.html

[13] H. Goldstein, *Classical Mechanics*, 2nd ed. New York: Addison-Wesley, 1980, pp. 114–118.

[14] E. L. Peterson, "Soft errors due to protons in the radiation belt," *IEEE Trans. Nucl. Sci.*, vol. NS-28, pp. 3981–3986, Dec. 1981.

[15] "Development and demonstration of a radiation tolerant 4M SRAM single-event-upset test report," Defense Threat Reduction Agency Report, July 9, 2001.

[16] J. S. Melinger *et al.*, "Critical-evaluation of the pulsed-laser method For single event effects testing and fundamental-studies," *IEEE Trans. Nucl. Sci.*, vol. 41, pp. 2574–2584, Dec. 1994.

[17] P. J. McNulty, W. G. Abdel-Kader, and G. E. Farrell, "Proton induced spallation reactions," *Radiat. Phys. Chem.*, vol. 43, no. 1/2, pp. 139–149, 1993.

[18] T. W. Armstrong *et al.*, "High energy transport code," *Nucl. Sci. Eng.*, vol. 49, pp. 82–95, 1972.

[19] J. Levinson *et al.*, "On the angular dependence of proton induced events and charge collection," *IEEE Trans. Nucl. Sci.*, vol. 41, pp. 2098–2102, Dec. 1994.

[20] P. E. Dodd *et al.*, "SEU-sensitive volumes in bulk and SOI SRAM's from first-principles calculations and experiments," *IEEE Trans. Nucl. Sci.*, vol. 48, pp. 1893–1903, Dec. 2001.

[21] J. R. Schwank *et al.*, "Anomalous charge collection from SOI substrates and its effect on SEU hardness," *IEEE Trans. Nucl. Sci.*, to be published.